ARMY RESEARCH LABORATORY

Modeling of Near-Field Blast Performance

by Barrie E. Homan, Matthew M. Biss, and Kevin L. McNesby

ARL-TR-6711 November 2013

NOTICES

Disclaimers

The findings in this report are not to be construed as an official Department of the Army position unless so designated by other authorized documents.

Citation of manufacturer's or trade names does not constitute an official endorsement or approval of the use thereof.

Destroy this report when it is no longer needed. Do not return it to the originator.

Army Research Laboratory

Aberdeen Proving Ground, MD 21005-5066

ARL-TR-6711 **November 2013**

Modeling of Near-Field Blast Performance

Barrie E. Homan, Matthew M. Biss, and Kevin L. McNesby

Weapons and Materials Research Directorate, ARL

REPORT DOCUMENTATION PAGE	Form Approved OMB No. 0704-0188

1. REPORT DATE *(DD-MM-YYYY)*	2. REPORT TYPE	3. DATES COVERED (From - To)
November 2013	Final	October 2012-September 2013

4. TITLE AND SUBTITLE
Modeling of Near-Field Blast Performance

5a. CONTRACT NUMBER

5b. GRANT NUMBER

5c. PROGRAM ELEMENT NUMBER

6. AUTHOR(S)
Barrie E. Homan
Matthew M. Biss
Kevin L. McNesby

5d. PROJECT NUMBER

5e. TASK NUMBER

5f. WORK UNIT NUMBER

7. PERFORMING ORGANIZATION NAME(S) AND ADDRESS(ES)
U.S. Army Research Laboratory
ATTN: RDRL-WMP-G
Aberdeen Proving Ground, MD 21005-5066

8. PERFORMING ORGANIZATION REPORT NUMBER
ARL-TR-6711

9. SPONSORING/MONITORING AGENCY NAME(S) AND ADDRESS(ES)

10. SPONSOR/MONITOR'S ACRONYM(S)

11. SPONSOR/MONITOR'S REPORT NUMBER(S)

12. DISTRIBUTION/AVAILABILITY STATEMENT
Approved for public release; distribution is unlimited.

13. SUPPLEMENTARY NOTES

14. ABSTRACT
Two hydrocode packages, ALE3D and CTH, were used to model the blast from a 450-g sphere of the near-ideal explosive composition 4. The pressure profile was optically measured using high-speed video and streak camera imaging techniques. Pressure profiles were obtained by measuring the velocity of the shock wave and using the Rankine-Hugoniot theory to calculate peak pressure. The high-resolution model results were compared to the optical data, standard gauge data, and the empirical blast estimation code CONWEP.

15. SUBJECT TERMS
ALE3D, CTH, Air Blast, C4

16. SECURITY CLASSIFICATION OF:			17. LIMITATION OF ABSTRACT	18. NUMBER OF PAGES	19a. NAME OF RESPONSIBLE PERSON
a. REPORT	b. ABSTRACT	c. THIS PAGE			Barrie E. Homan
Unclassified	Unclassified	Unclassified	UU	20	19b. TELEPHONE NUMBER (*Include area code*) 410-306-0932

Standard Form 298 (Rev. 8/98)
Prescribed by ANSI Std. Z39.18

Contents

List of Figures

List of Tables

INTENTIONALLY LEFT BLANK.

1. Introduction

The characterization of explosive performance has historically concentrated on the detonation wave within the material and the blast wave generated in the far field. The far field is defined here as any distance after which the air shock wave has separated from the detonation product cloud. By this point, the energy within the explosive can no longer contribute to the air shock, and further air shock propagation depends only on the local properties of the ambient air. An alternate criteria for delineating the far field is the position of the air shock/fireball interface at the time the detonation products "freeze out" and no longer react (*1*). The freeze-out temperature is chosen by comparison of calorimetry experiments (*2, 3*) and thermoequilibrium calculations using CHEETAH (*4*). The near field is defined here as the region between the original charge surface and the position of the air shock wave when it has separated from the fireball surface. Little information is available concerning the near-field region of an explosive event mainly due to the experimental difficulty in measuring its characteristics (*5*). Standard blast gauge data suffers from thermal loading and slow response times making mechanical measurements unreliable (*6*). Before the shock wave has decoupled from the fireball, the motion in different density fluids, detonation products and air, lead to instabilities that distort the contact surface between the products and undisturbed air. The Richtmyer-Meshkov (*7*) and Rayleigh-Taylor (*8*) instabilities have been identified (*9*) as the two main mechanisms at work. These mechanisms can significantly affect the pressure profile when measured along any one particular radial direction.

Munition case fragmentation and subsequent fragment acceleration behaviors are mainly a function of the detonation wave characteristics and early expansion (*10*) and are reasonably described by the Gurney theory (*11*). For ideal explosives, defined by instantaneous chemical kinetics at the detonation front (*12*), the detonation wave is driven by the residual thermal energy contained by the detonation products. Because all explosives show some degree of nonideality, (*13*) the detonation wave is affected by the finite-rate chemistry that can occur later in the explosion process. The after-burning process, enhanced when incorporating the surrounding oxygen in the atmosphere, can significantly affect the blast performance of explosive materials (*14*).

The near-field, far-field demarcation can be seen in the series of high-brightness (*1*) shadowgraph images from a detonation of a 2-kg cylinder of TNT (trinitrotoluene), depicted in figure 1. Before approximately $391\,\mu s$, the air shock cannot be seen as it is integrated with the fireball. After $391\,\mu s$, the air shock pulls away from the product cloud as the shock enters the far-field

region. At this point, the explosive chemistry no longer plays a role in determining the air shock strength as that wave travels farther away from the event.

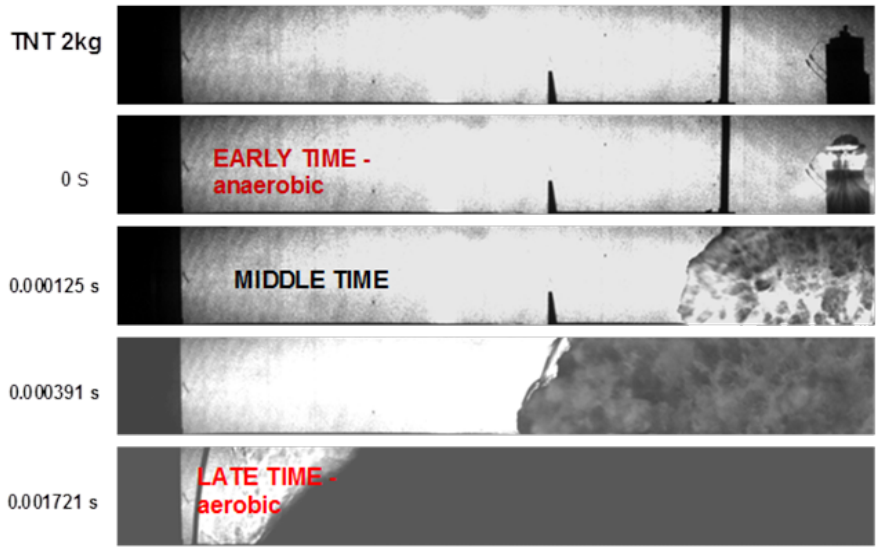

Figure 1. TNT blast field.

To determine the fidelity of the various modeling tools available, the ALE3D (*15*) and CTH (*16*) hydrocode families are used to model the detonation of a 450-g sphere of the plastic-bonded explosive (PBX) Composition 4 (C4) (92% cyclotrimethylenetrinitramine [RDX] and remainder plasticizer/binder). These results are compared to experiments and the semi-empirical one-dimensional blast code CONWEP (*17*). The CONWEP code attempts to determine the shock wave pressure as a function of distance from a charge based on a set of equations and empirical curves of explosives developed in the 1940s. Because the data was collected in the far field limit, caution should be exercised when extrapolating to the near field regime.

2. Models

Two Department of Energy hydrodynamic simulation codes were used in this study. The CTH (*16*) code is from Sandia National Laboratory and is based on a pure Eulerian mesh model. The ALE3D (*15*) code from Lawrence Livermore National Laboratory can also use an Arbitrary Eulerian/Lagrangian mesh model (the ALE in ALE3D), but for consistency, it was restricted to pure Eulerian mode in this study. The model parameters used in the simulation are given in table 1. The solid C4 was treated hydrodynamically (no strength), and the Jones-Wilkins-Lee (JWL)

model (*18*) was used for the detonation products equation of state (EOS) in conjunction with the programmed-burn detonation model. The programmed-burn model assumes instantaneous kinetics by implementing the product JWL EOS at the appropriate time calculated strictly as a function of the distance from the initiation point. The mesh had axisymmetric geometry and showed reasonable convergence with a (square) cell resolution of 20 nodes/cm as evidenced by stable solution with mesh refinement.

Table 1. JWL model parameters.

Parameter	**Value**
A	6.098 Mbar
B	0.1295 Mbar
R_1	4.5
R_2	1.4
ω	0.25
Density, ρ	1.601 g/cm^3
Detonation Velocity, D	0.8193 cm/μs

3. Experimentation

The peak shock wave pressure was measured from the surface of a top-detonated sphere of C4 and is depicted in figure 2 (*19*). In figure 2a, experimental images from a 450-g sphere that is detonated directly with an RP-83 detonator are shown. In figure 2b, images of pressure contours from an ALE3D calculation are shown for comparison. The pressure map of the event can be directly determined from the calculation as it is one of the fundamental quantities tracked by the codes. As figure 2b represents a two-dimensional map, the pressure inside the charge itself can also be determined giving a clearer picture of the detonation wave behavior. To measure the pressure experimentally, the shock wave position was mapped in time and converted to velocity. Based on the Rankine-Hugoniot theory (*20*) in which the conservation equations (mass, momentum, and energy) must be satisfied, the peak shock pressure can be related to the velocity of the air shock by (*12*):

$$P = F(\gamma)(M^2 - 1)P_0$$
$$F(\gamma) = \frac{2\gamma}{\gamma + 1}, \gamma = \frac{C_p}{C_v} \quad (1)$$

where *M* is the shock wave Mach number defined as the ratio of the shock velocity to the ambient speed of sound, and C_p and C_v are the heat capacities at constant pressure and volume, respectively. For peak pressures less than ~4 MPa, the use of the gamma law equation of state with $\gamma = 1.4$ can be reasonably used giving *F* as $7/6$ or 1.17 (*12*). Because *F* is a slowly varying function of gamma, equation 1 predicts shocks traveling within the explosive products ($\gamma \approx 1.23 \implies F = 1.10$) at the equivalent velocities, will have peak pressures approximately 5% lower than that from the purely air shocks. Once the shock wave has separated from the fireball, the shock is readily apparent from the optical data and gamma can be safely held constant at 1.4. Equation 1 also assumes that there is no chemical energy release at the shock front, and that assumption is satisfied in the far field after shock separation. Before this time, however, the shock is assumed to coincide with the leading edge of the fireball (*21*). Based on thermochemical calculations (*4*) the energy release from the C4 detonation is complete when the fireball diameter reaches ~ 1.26 of the original charge diameter as this explosive is near-ideal. Except for very near the charge surface, the assumptions behind equation 1 as used here (no energy release, constant γ, assumed ambient sound speed) are reasonable approximations.

The experimental setup is detailed elsewhere (*19*) and will only be outlined here. The C4 charge was placed within the indoor blast chamber at the U.S. Army Research Laboratory facility located at Aberdeen Proving Ground, MD. The charge was top detonated using an RP-83 detonator with no booster. Optical diagnostics as well as wall and bar gauges were used to measure the pressure with only optical measurement results being reported here. The one-dimensional high-speed streak camera (Photron SA-5) used to measure the shock velocity was operated at 0.7 million frames per sec (Mfps) with an exposure of 370 ns. This was compared to a framing camera (Cordin Co. Model 570) that was operated at 2.5 Mfps with an exposure of 300 ns. The high-speed camera had a field of view that would encompass most of the expansion of the blast, whereas the framing camera was trained on the region close to the charge surface. The optical techniques used here were restricted to measuring the shock wave position along one radius. The calculations performed in this work, experimental measurements (*22*), and calculations of others (*9*) agree that there are variations in the temporal position of the shock front as a function of azimuthal angle mainly due to nonconcentric initiation points and inherent instabilities as mentioned in the introduction.

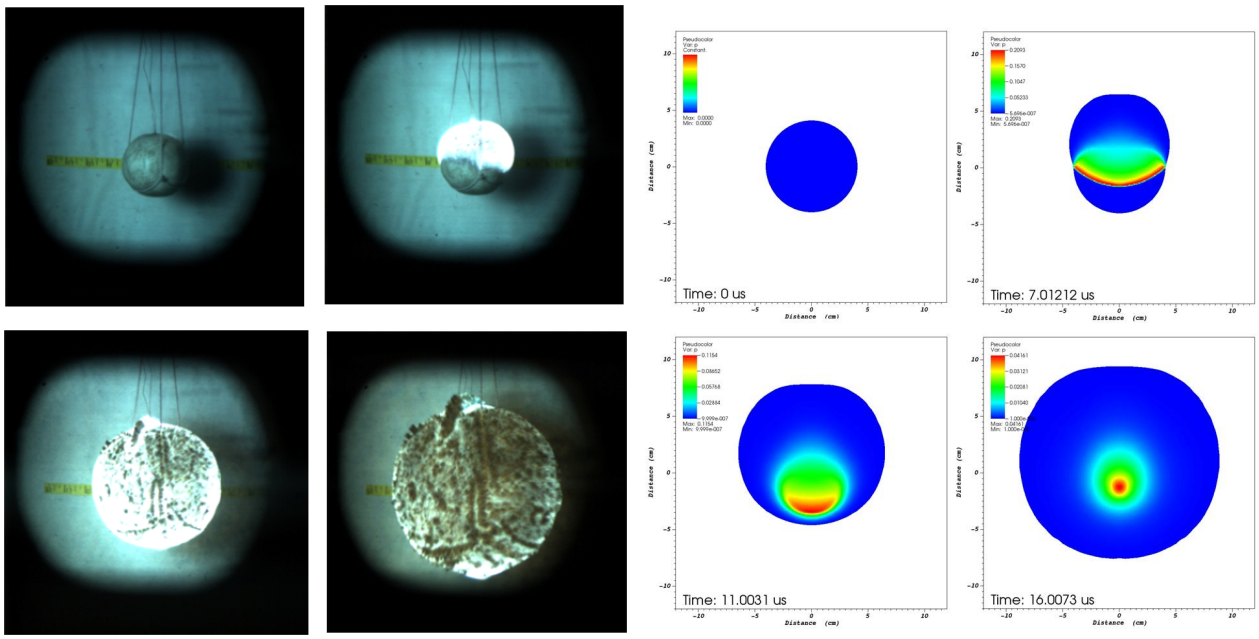

(a) (b)

Figure 2. Experiment (a) and ALE3D model (b) of 450 g of C4.

4. Results

Measurement of the shock position as a function of time using the streak camera instrument is shown in figure 3. The Photron camera software was used to determine the distance from the charge surface with an image resolution of 0.2 mm per pixel. Results for the CTH and ALE3D models are shown in figure 3 for comparison. Excellent agreement can be seen between the two model packages with reasonable agreement with experiment. However, to use equation 1, the derivative of the position data is required. Simple differencing of the distance-time curve in figure 3 proved noisy, so a third-order polynomial was fitted to the experimental distance vs. time data. This polynomial function, with parameters given in table 2, was then differentiated following a standard Savitzky-Golay scheme (*23*) to obtain the velocity data. Figure 4 shows the velocity results in one radial direction from the two optical instruments, the empirical calculation CONWEP (*17*), and results from the two hydrodynamic codes. The experimental data and the hydrocode model sampling were taken in a direction $90°$ from the detonation point. The Photron camera diverges significantly from the Cordin imaging technique at the higher pressures corresponding to higher shock velocities. This is attributed to the lower resolution (spatial and temporal) of the Photron instrument. Farther out from the charge surface, the three models agree

reasonably well with the data from the Photron camera. Near the original charge surface, the ALE3D and CONWEP calculations appear to support the higher velocities measured by the Cordin system. The discrepancy between $\sim$50 mm and 100 mm from the charge surface from the ALE3D calculations and the Cordin optical data could be attributed to the resolution of the model mesh in this region and is the subject of future refinement. This is the region in which the shock wave is transitioning from the driven detonation wave from the solid to gas phase propagation, as evidenced by the higher deceleration in this region as compared to further out. The rarefaction wave that has been generated at the solid-air interface will also contribute to the decrease in shock pressure and subsequent velocity decrease.

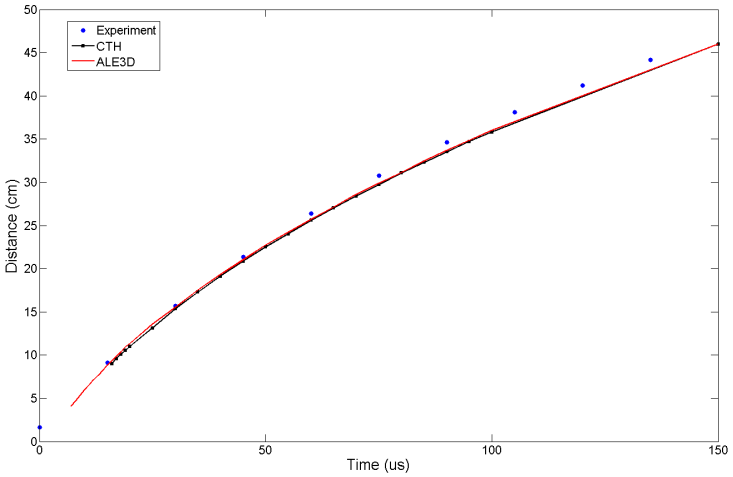

Figure 3. Shock distance from surface of a 450-g C4 charge.

Table 2. Third-order polynomial parameters.

Term	**Coefficient**
t^3	5.0×10^{-5} mm^3/μs
t^2	-2.27×10^{-2} mm^2/μs
t	5.30 mm/μs
constant	16.71 mm

The experimental velocities in figure 4 were then converted to pressures using equation 1 and plotted in figure 5 along with direct pressure calculations using the hydrocodes. The pressure region, corresponding to the region in which the velocity profiles had less agreement (figure 4

50 and 100 mm) shows similar disagreement in pressure. This may be due to the the resolution of both the experiments and models and/or effects from the flow instabilities mentioned earlier in the introduction. The three models compare favorably with each other and, except for this transition region, were in reasonable agreement with the experimental data.

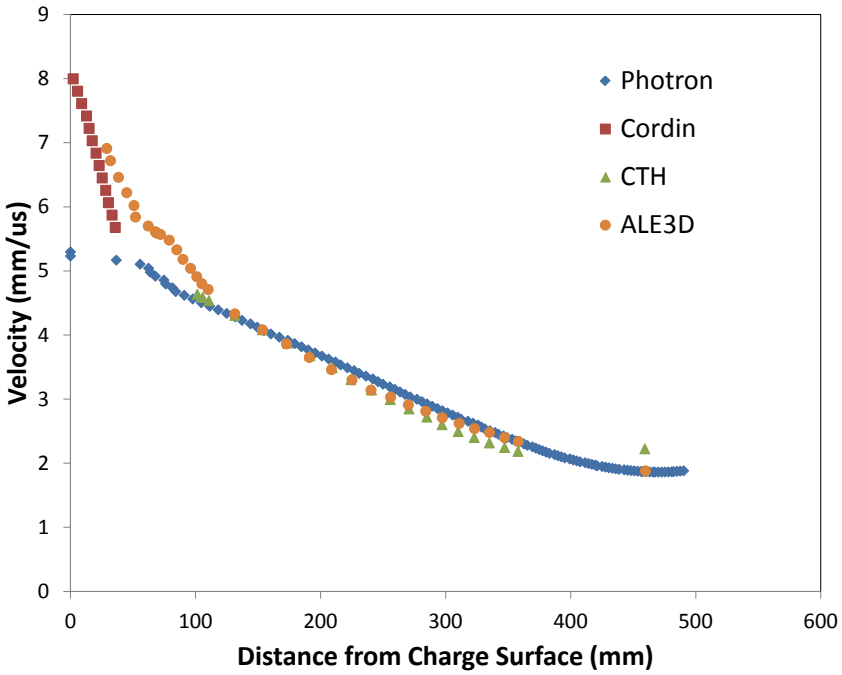

Figure 4. Shock velocity comparison.

5. Conclusions

Modeling of the near-field blast pressures from 450-g spheres of the explosive C4 have been conducted using three modeling packages: CONWEP, ALE3D, and CTH. The calculations were compared to experimental optical measurements of the pressures obtained by application of the Rankine-Hugoniot theory (*20*). For most radial distances, very good agreement has been obtained between the models and the models with experiments. Both experiments and models suggest that close to the original charge surface, a transition from one propagation scenario to another is taking place and this region needs further study. The overall agreement leads credence to the notion that optical pressure measurements can be used to map out the shock pressure fields of an explosive event from near the charge surface where traditional gauges are less effective to far-field distances where comparison with gauges are a reasonable check on the model

parameters. Better differentiation techniques would enhance the velocity resolution and hence the pressure fidelity.

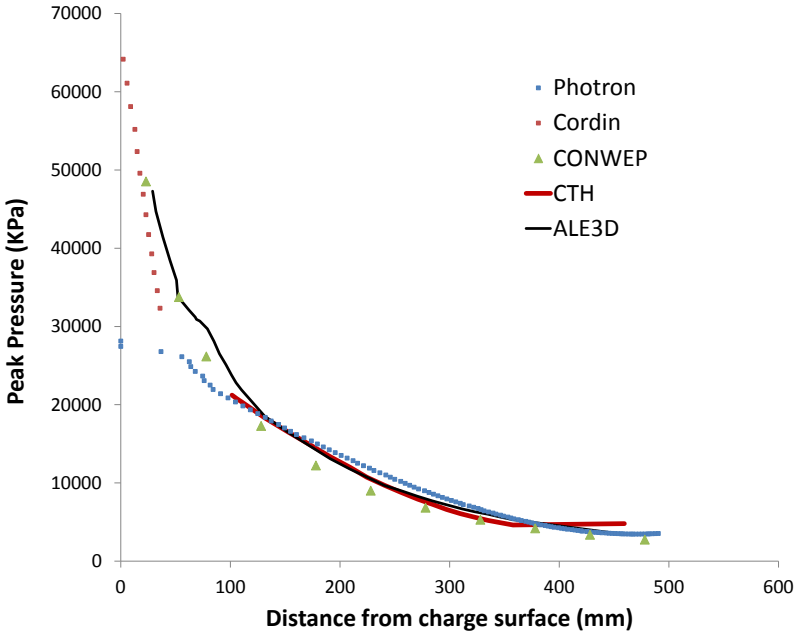

Figure 5. Shock peak pressures. Pressure error estimated at $\pm$ 10%.

6. References

1. McNesby, K. L.; Homan, B.; Lottero, R. *High Brightness Imaging for Real Time Measurement of Shock, Particle, and Combustion Fronts Produced by Enhanced Blast Explosives*; ARL-TR-3411; U.S. Army Research Laboratory: Aberdeen Proving Ground, MD, 2005.

2. Bastea, S.; Fried, L. *Chemical Equilibrium Detonation*; volume 6 of *Shock Wave Science and Technology Reference Library* Springer: NY, 2012.

3. Ornellas, D. *Calormetric Determination of the Heat and Products of Detonation for Explosives*; UCRL-52821; Lawrence Livermore National Laboratory: Livermore, CA, 1982.

4. Bastea, S.; Fried, L.; Glaesemann, K.; Howard, W.; Kuo, I.; Souers, P.; Vitello, P. *CHEETAH Users Manual*; Lawrence Livermore National Laboratory: Livermore, CA, 2012.

5. Walter, P. *Introduction to Air Blast Measurements - Part I*; PCB Tech Note TN-12; PCB Piezotronics, Inc.: Depew, NY, 2004.

6. Eaton, W.; Smith, J. Micromachined Pressure Sensors: Review and Recent Developments. *Smart Material Structures* **1997**, *6*, 530-539.

7. Brouillette, M. THE RICHTMYER-MESHKOV INSTABILITY. *Annual Review of Fluid Mechanics* **2002**, *34* (1), 445-468.

8. Taylor, G. The Instability of Liquid Surfaces When Accelerated in a Direction Perpendicular to their Planes. I. *Proceedings of the Royal Society of London. Series A. Mathematical and Physical Sciences* **1950**, *201* (1065), 192-196.

9. Klomfass, A. Numerical Analysis of Fluiddynamic Instabilities and Pressure Fluctuations in the Near Field of a Detonation. In *Predictive Modeling of Dynamic Processes*; Hiermaier, S., Ed.; Springer US: New York, NY, 2009; pp 239–259.

10. Cooper, P. *Explosives Engineering*; Wiley-VCH: NY, 1996.

11. Gurney, R. *The Initial Velocities of Fragments from Bombs, Shells, and Grenades*; BRL-405; Ballistic Research Laboratory: Aberdeen Proving Ground, MD, 1943.

12. Needham, C. *Blast Waves*; Springer: NY, 2010.

13. Mader, C. *Numerical Modeling of Explosives and Propellants, 3rd ed.*; CRC Press: Boca Raton, FL, 2008.

14. McNesby, K.; Homan, B.; Ritter, J.; Quine, A.; Ehlers, R.; McAndrew, B. Afterburn Ignition Delay and Shock Augmentation in Fuel Rich Solid Explosives. *Propellants, Explosives, and Pyrotechnics* **2010**, *35* (1), 57-65.

15. Nichols, A. *Users Manual for ALE3D: An Arbitrary Lagrangian/Eulerian 2D and 3D Code System*; LLNL-SM-433954; Lawrence Livermore National Laboratory: Livermore, CA, 2010.

16. Crawford, D.; Brundage, A.; Harstad, E.; Hertel, E.; Schmitt, R.; Schumacher, S.; Simmons, J. *CTH User's Manual and Input Instructions*; Sandia National Laboratory: Albuquerque, NM, 2011.

17. Hyde, D. W. *Microcomputer Programs CONWEP and FUNPRO, Applications of TM 5-855-1, "Fundamentals of Protective Design for Conventional Weapons" (User's Guide)*; SL-88-1; Army Engineer Waterways Experiment Station, Structures Laboratory: Vicksburg, MS, 1988.

18. Bobratz, B.; Crawford, P. *LLNL Explosives Handbook*; UCRL-52997; Lawrence Livermore National Laboratory: Livermore, CA, 1985.

19. McNesby, K.; Biss, M.; Benjamin, R.; Thompson, R. *Optical Pressure Measurements of Explosions*; ARL-TR-6488; US Army Research Laboratory: Aberdeen Proving Ground, MD, 2013.

20. Kinney, G.; Graham, K. *Explosive Shocks in Air, 2nd ed.*; Springer-Verlag: Berlin, 1985.

21. McNesby, K. L.; Homan, B. *Real-Time Optical Measurements for Improved Understanding of Enhanced Blast Materials*; ARL-TR-3483; U.S. Army Research Laboroatory: Aberdeen Proving Ground, MD, 2005.

22. Sutherland, G. T.; Boyle, V.; Benjamin, R.; Biss, M. *Near Field Pressure and Visualization Experiments for Composition C4 and Pentolite Spherical Charges*; ARL Technical Report In Press; US Army Research Laboratory: Aberdeen Proving Ground, MD, 2013.

23. Savitzky, A.; Golay, M. Smoothing and Differentiation of Data by Simplified Least Square Procedure. *Analytical Chemistry* **1964**, *85* (8), 1627-1639.

NO. OF COPIES	ORGANIZATION
1 (PDF)	DEFENSE TECHNICAL INFORMATION CTR DTIC OCA
1 (PDF)	DIRECTOR US ARMY RESEARCH LAB IMAL HRA
1 (PDF)	DIRECTOR US ARMY RESEARCH LAB RDRL CIO LL
1 (PDF)	GOVT PRINTG OFC A MALHOTRA

NO. OF COPIES	ORGANIZATION
	ABERDEEN PROVING GROUND
16 (PDF)	DIR USARL RDRL SLB W P GILLICH C KENNEDY RDRL WMP S SCHOENFELD RDRL WMP A R MUDD RDRL WMP B C HOPPEL RDRL WMP C T BJERKE RDRL WMP D J RUNYEON RDRL WMP E P SWOBODA RDRL WMP F E FIORAVANTE N GNIAZDOWSKI RDRL WMP G R BANTON N ELDREDGE B HOMAN B KRZEWINSKI S KUKUCK J STEWART

NO. OF COPIES	ORGANIZATION